First Experiments on 3D Plasma Calculations Using Positive Maxwellian Operator

Volodymyr E. Moiseenko [1,2*], *Nikita* Skhabytskyi[1], and *Yurii* Martseniuk[1]

[1]Institute of Plasma Physics, National Science Center "Kharkiv Institute of Physics and Technology", 61108, Kharkiv, Ukraine
[2]Uppsala University, S-75108 Uppsala, Sweden

Abstract. A new form of time-harmonic Maxwell's equations [1] based on the standard formulation is used for the numerical modelling of RF fields in non-uniform plasmas without an external magnetic field. This formulation expresses the equations in terms of magnetic field strength, electric displacement, the vector and scalar potential. It offers several advantages. First, the differential operators act directly on these quantities with positive definiteness. Second, curl operators are absent in the leading-order terms of the equations. The Laplacian appears as the leading-order operator in the equations for potentials and magnetic field, while the gradient of a divergence is the leading-order operator for the electric displacement. Third, the absence of spatially varying coefficients in the leading-order differential operators ensures diagonal dominance of the discretized matrix. Following the approach of [1], the computational domain is chosen as a rectangular parallelepiped. A lowest-order 3D finite-difference method is applied for discretization. The antenna model is represented by a divergence-free electric current directed along the y axis. The plasma is treated as three-dimensional, non-uniform, and unmagnetized.

1 Introduction

While the standard discretization methods for time-harmonic Maxwell's equations – such as Fourier transformations, the finite element method and the finite difference method, are well-established for deriving approximate solutions, they require substantial computational resources, including large amounts of RAM (random access memory) and FLOPS (floating point operations per second), making them computationally intensive. As a result, these methods often rely on high-performance computing systems, such as supercomputers, to execute simulations.

Additionally, these computing approaches are inefficient when applied to Maxwell's equations. However, there is a consistent need for some form of solution, either exact or approximate for applied physics, especially using commonly available computing resources.

To address the computational demands, [1] proposes an alternative approach that reduces memory requirements when implemented with the CG (conjugate gradient) method. Numerical tests demonstrated that fast convergence could be achieved without preconditioning, with only a reasonable number of iterations.

The method described in [1] was validated in test conditions but has not been evaluated in media with spatially varying properties. This study aims to assess the features of the proposed formulation in such environments, specifically with space-varying plasma media.

2 Numerical model

2.1 Positive-definite Maxwellian operator

Proposed by [1], the form of time-harmonic Maxwell's equations is expressed as:

$$\begin{aligned}
&-\nabla(\nabla\cdot\mathbf{D}) + k_0^2\left(\hat{I}+\hat{\zeta}^{*T}\cdot\hat{\zeta}\right)\cdot\mathbf{D}\\
&-k_0^2\hat{\zeta}^{*T}\cdot\mathbf{A} - ik_0\nabla\times\mathbf{H} - ik_0\hat{\zeta}^{*T}\cdot\nabla\Phi = -ik_0\tfrac{4\pi}{c}\mathbf{j} - 4\pi\nabla\rho,\\
&-\nabla^2\Phi + ik_0\nabla\cdot\mathbf{A} - ik_0\nabla\cdot\left(\hat{\zeta}\cdot\mathbf{D}\right) = 0,\\
&-\nabla^2\mathbf{H} + k_0^2\mathbf{H} + ik_0\nabla\times\mathbf{A} + ik_0\nabla\times\mathbf{D} = \tfrac{4\pi}{c}\nabla\times\mathbf{j},\\
&-\nabla^2\mathbf{A} + k_0^2\mathbf{A} - ik_0\nabla\times\mathbf{H} - k_0^2\hat{\zeta}\cdot\mathbf{D} + ik_0\nabla\Phi = 0,
\end{aligned} \tag{1}$$

In here, **D** is the electric displacement, $\Phi = \varphi/ik_0$ is the normalized scalar potential, **H** is the magnetic field strength, $\mathbf{A} = ik_0\mathbf{a}$ is the normalized vector potential, $\hat{I}$ is the identity tensor, $\hat{\zeta} = \hat{\varepsilon}^{-1}$ is the inverse media dielectric permittivity tensor, **j** is the external (antenna) current density, ρ is the charge density caused by **j**, and $k_0 = \omega/c$ is the wave number, where ω is the field frequency and c is the speed of light.

For further use, equations (1) are expressed explicitly as an operator acting on a vector:

$$\hat{M}\mathbf{x} = \mathbf{y}, \tag{2}$$

In here, $\hat{M}$ is the differential operator of the left-hand side of (1), and $\mathbf{x} = (D_x, D_y, D_z, \Phi, H_x, H_y, H_z, A_x, A_y, A_z)$ is the vector of unknowns in the left-hand side of equations (1), while **y** is the vector comprising the right-hand side of (1).

The positiveness of the operator $\hat{M}$ means $\left(\mathbf{x}, \hat{M}\mathbf{x}\right) = \int \mathrm{d}V\, \mathbf{x}^*\cdot\hat{M}\mathbf{x} > 0$ for any **x** vector of the

* Corresponding author: volodymyr.moiseyenko@angstrom.uu.se

domain, it is an inherent trait, which was proven within the scope of [1] for arbitrary dielectric medium permittivity, including a case of plasma without magnetic field which is considered here.

2.2 Boundary conditions

As a domain for the problem, a metallic parallelepiped cavity is chosen whose inner region is set by limiting an area of space to a finite volume:

$$x \in [0, l_x], y \in [0, l_y], z \in [0, l_z] \Rightarrow V = l_x \times l_y \times l_z.$$

For the boundary-value problem, equations (1) are paired with boundary conditions that are similar to those expressed within article [1]: The normal component of electric displacement **D** and vector potential **A** have Neumann boundary conditions, and their tangential components have Dirichlet boundary conditions. For the magnetic field strength **H**, the conditions are put in the opposite way: the normal component obeys the Dirichlet boundary conditions, and the tangential component has Neumann boundary conditions. The normalized scalar potential Φ has Dirichlet boundary conditions at all boundaries.

3 Currents and medium

For computational purposes, different expressions to article [1] are chosen for external current density and media dielectric permittivity. Both are chosen to satisfy the said boundary conditions.

3.1 External current density

The chosen expression for current density describes a single-strap antenna oriented in the y direction with current density distribution shaped as a bi-quadratic cosine in the x and z directions:

$$\mathbf{j}_a = I_a \frac{f(x)f(z)}{\delta_{a,x}\delta_{a,z}} \mathbf{e}_y, \quad (3)$$

In here, I_a is the antenna total current, $\delta_{a,x}$ and $\delta_{a,z}$ are half-widths of the antenna along the x and z direction, both $f(x)$ and $f(z)$ are described with the same function that shares a bell-like shape, but both differ in function parameters.

The chosen expressions for functions $f(x)$ and $f(z)$ are:

$$f(h) = \begin{cases} \cos^2\left(\frac{\pi[h-h_a]}{2\delta_{a,h}}\right) \text{ if } |h - h_a| \le \delta_{a,h}, \\ 0 \text{ if } |h - h_a| > \delta_{a,h}, \end{cases} \quad (4)$$

In here, h_a is x or z, the central coordinates of antenna, $\delta_{a,h}$ is the half-width of the antenna and h can be either x or z.

Expressions (3) and (4) are chosen to provide no dependence on y component, which in turn results in no net accumulation of the electric charge. The antenna current is explicitly independent of y, producing y-invariant source.

3.2 Media dielectric permittivity

The chosen expression for dielectric permittivity will describe a plasma-like medium inside the cavity:

$$\hat{\varepsilon} = \left[1 - \varepsilon_0 \sin(k_x x) \sin(k_y y) \sin(k_z z)\right]\hat{I}, \quad (5)$$

In here, ε_0 is the permittivity parameter, and k_x, k_y and k_z are the constants.

To model plasma-like medium, the second term in (5) is chosen to be positive. Therefore, the constants k_x, k_y and k_z within the arguments of the sines must be chosen accordingly:

$$k_x = \frac{\pi}{l_x}, k_y = \frac{\pi}{l_y}, k_z = \frac{\pi}{l_z}, \quad (6)$$

In here, l_x, l_y, and l_z are lengths of parallelepiped metal cavity.

Rather than using permittivity (5), its inverse is used in this research:

$$\hat{\zeta} = \frac{1}{1 - \varepsilon_0 \sin(k_x x) \sin(k_y y) \sin(k_z z)} \hat{I}, \quad (7)$$

In present calculations the parameter ε_0 is chosen to be less then unity to avoid singularity in (7).

4 Discretization

Discretization of the described system is done using the low order finite differences method. For simplicity, the mesh is uniform. The numbers of nodes (N_x , N_y and N_z) are to be prescribed for each direction independently. After discretization, the system is then eligible for computation using the CG method.

5 Numerical solution

5.1 Parameters of numeric experiment

In our numerical experiments, the parallelepiped metal cavity has dimensions $l_x = l_y = 24$ [cm], $l_z = 100$ [cm], with the number of nodes in a mesh $N_x = N_y = 49$, $N_z = 201$. This mesh and these dimensions are chosen because they produce results with observable wavelengths in the case of vacuum and plasma fillings.

A single-strap antenna defined with expressions (3) and (4) has dimensions $\delta_{a,x} = 2$ [cm] and $\delta_{a,z} = 10$ [cm], is centered at coordinates $(x_a, z_a) = (6$ [cm], 25 [cm]) and has a total antenna current $I_a = 2997924536.8$ [stA].

The chosen frequency for fields is $\omega = 6.3 \times 10^9$ [s^{-1}], which belongs to the UHF range.

Calculations are performed for vacuum and plasma cases (see, e.g. [2]), which correspond to permittivity parameter ε_0 values of 0.0 and 0.9. Recalling the cold dielectric medium permittivity of collisionless plasma:

$$\varepsilon(\omega) = 1 - \frac{\omega_{pe}^2}{\omega^2}, \omega_{pe} = |e|\sqrt{\frac{4\pi n_e}{m_e}}, \quad (8)$$

In here, ω_{pe} is the plasma frequency, n_e is the electron density, m_e is the electron mass, e is the electron charge.

Peak plasma frequency $\omega_{pe} = 5.9 \times 10^9$ [s^{-1}] can be found from $\varepsilon_0 = 0.9$, and corresponds to $n_e = 1.1 \times 10^{10}$ [cm^{-3}].

5.2 Experiment results

Only Im{**D**}, Re{Φ}, Re{**H**} and Im{**A**} field parts are non-zero, based on the observation about real external current density and dielectric permittivity.

5.2.1 Vacuum case

Computation for vacuum yield results in field components that correspond to the WKB approximation method.

The calculated solution for vacuum yields only one real vector field, which is the magnetic strength field, displayed in Figures 1 and 2.

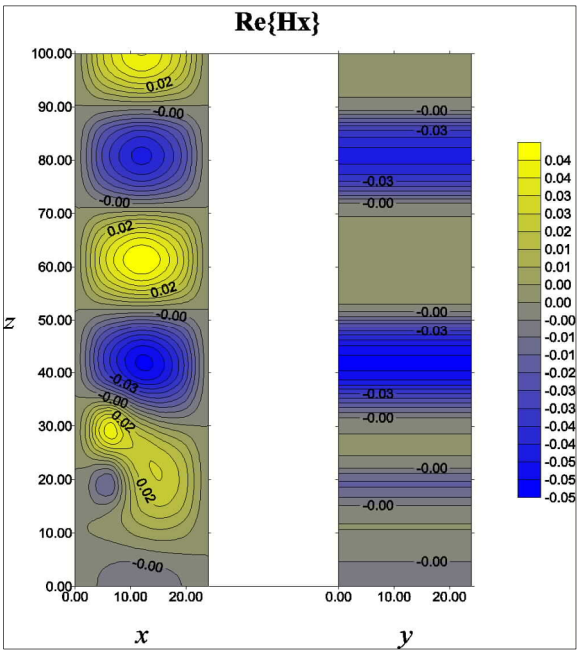

Fig. 1. Real part of H_x component in vacuum medium in x0z and y0z central cross-sections.

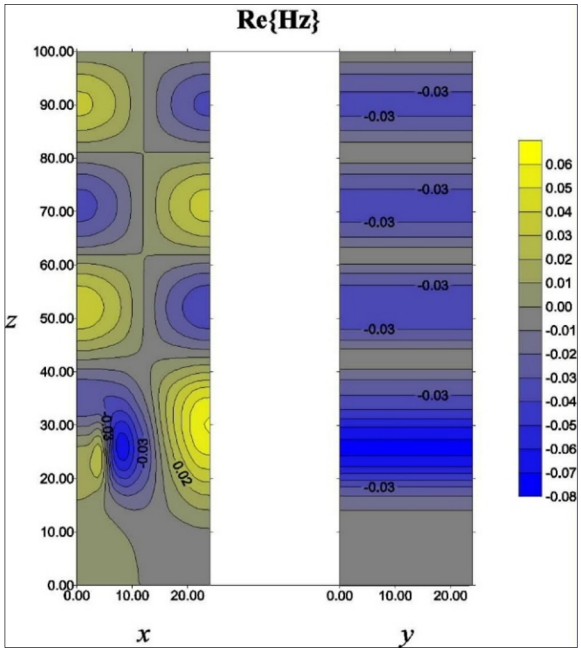

Fig. 2. Real part of H_z component in vacuum medium in x0z and y0z plains.

Figures 1 and 2 show no dependence on the y coordinate, which aligns with expressions (3) and (4) and corresponds to the normalized scalar potential of zero. The field distribution resembles the $TE_{1,0,5}$ mode of a rectangular cavity, with 1 observed half-wavelength in the x direction, 0 half-wavelengths in the y direction, and 5 half-wavelengths in the z direction (3 of which are visible and 2 of which are distorted by the antenna field), indicating that the vacuum cavity behaves as a resonator that supports this mode. This trait appears for all non-zero components of the field in a vacuum. Recalling an expression for the natural frequency of a vacuum parallelepiped metal resonator:

$$\omega_{i,j,k} = \pi c \sqrt{(i/l_x)^2 + \left(j/l_y\right)^2 + (k/l_z)^2}\,. \quad (9)$$

In here, $\omega_{i,j,k}$ is the natural frequency, i, j and k are natural numbers, l_x, l_y and l_z are lengths of parallelepiped metal cavity.

The natural frequency $\omega_{1,0,5} = 6.1\times10^9$ [s^{-1}], which is quite close to the field frequency.

Additionally, the calculated solution for vacuum yields two imaginary vector fields, which are electric induction and normalized vector potential fields, displayed in Figure 3.

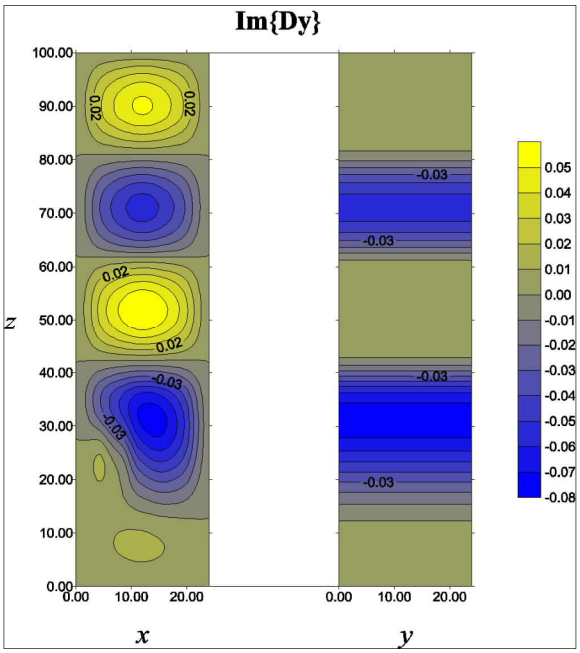

Fig. 3. Imaginary part of D_y and A_y components in vacuum medium in *x0z* and *y0z* plains.

It is worth noting that Figure 3 depicts the same values for D_y and A_y due to normalized scalar potential being zero throughout the calculation domain.

5.2.2 Plasma case

To ensure consistency in comparison, the same field components – considered in their respective real and imaginary parts – are used.

The calculated solution for the real part of the magnetic strength field is displayed in Figures 4 and 5. Cross-referencing Figures 1 and 2 with Figures 4 and 5 shows that the ever-present antenna field is rather more visible in plasma calculations. Along with this, field dependence on y makes an appearance. The emergence of y-dependence in the field structure is primarily due to the 3D non-uniformity of the plasma, not the antenna geometry. Hence, the observed y-dependence is a direct consequence of the plasma inhomogeneity,

demonstrating the capability of the method to capture symmetry-breaking effects in 3D media.

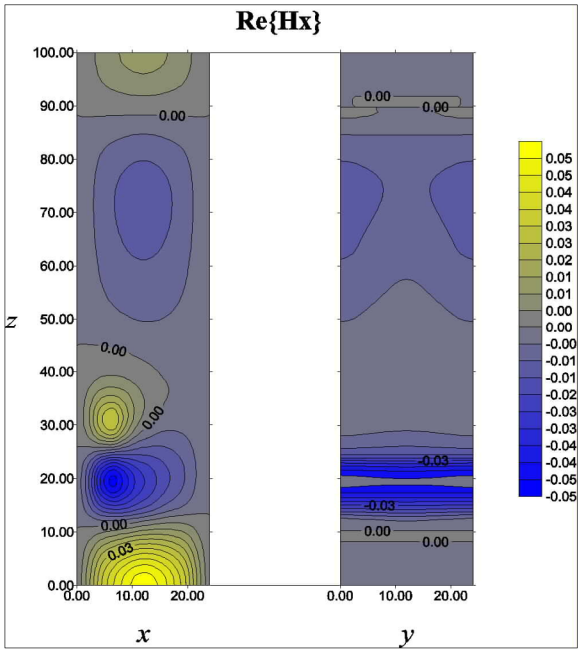

Fig. 4. Real part of H_x component in plasma medium in *x0z* and *y0z* plains.

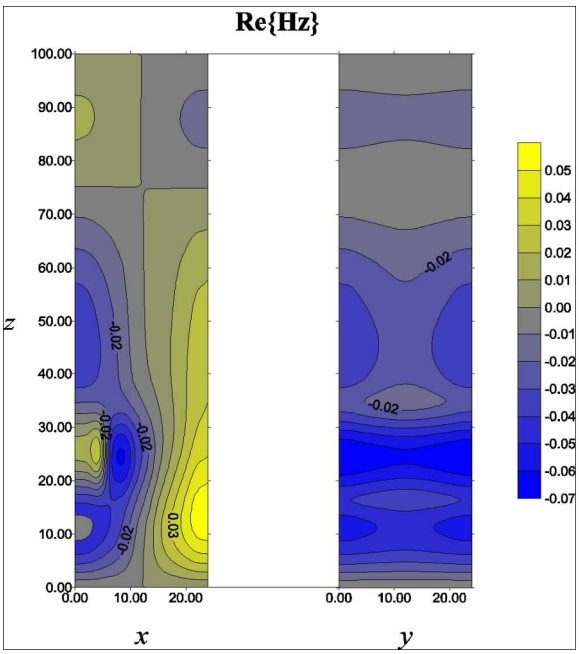

Fig. 5. Real part of H_z component in plasma medium in *x0z* and *y0z* plains.

The physically more pronounced field of the single-strap antenna means that natural modes amplify less because the difference between natural frequency and field frequency becomes greater, which is also evident by visible elongation of the wavelength compared to a case of vacuum.

Calculated solution for imaginary parts of electric displacement and normalized vector potential in plasma medium, is displayed in Figures 6 and 7.

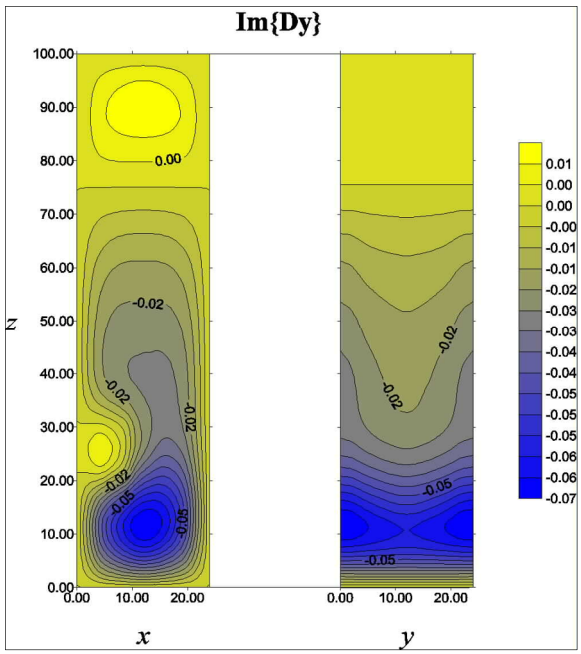

Fig. 6. Imaginary part of D_y component in vacuum medium in *x0z* and *y0z* plains.

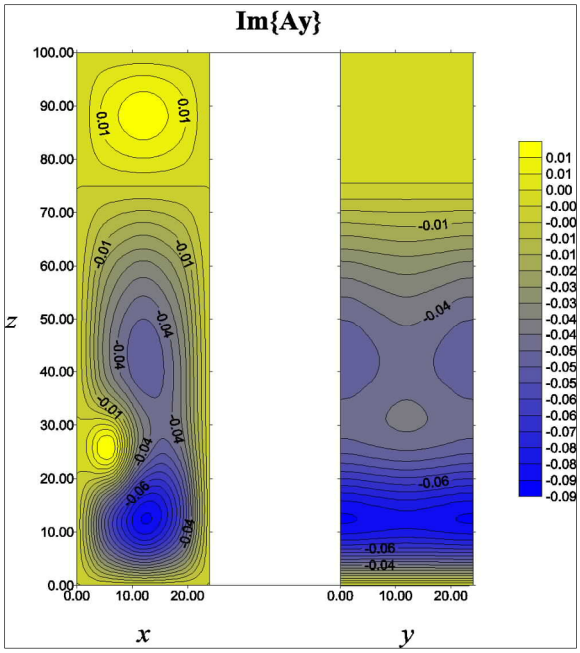

Fig. 7. Imaginary part of A_y component in vacuum medium in *x0z* and *y0z* plains.

The dominance of antenna-driven fields over cavity resonances in the plasma case is primarily due to resonant frequency detuning, rather than power absorption. In vacuum, the driving frequency $\omega = 6.29\times10^9$ s^{-1} is very close to the natural frequency of the $TE_{1,0,5}$ mode $\omega_{1,0,5} = 6.1\times10^9$ s^{-1}, leading to increase of amplitude of $TE_{1,0,5}$. When plasma is introduced, the effective permittivity decreases ($\varepsilon < 1$), which increases the phase velocity and shifts the resonant frequencies upward. This increases the distance between the driving frequency and the nearest cavity mode, decreasing resonant amplification. Thus, the system transitions from a resonance-dominated regime (vacuum) to a driven, non-resonant regime

(plasma), making the direct antenna near-field more prominent relative to standing cavity modes.

In plasma, electric displacement shows enhanced amplitude near the antenna, indicating strong capacitive coupling and reactive near-field effects. It reflects energy storage in the electric field rather than dissipation.

These results are consistent across all calculated fields. This observation reinforces the physical consistency of the system and confirms the applicability of equations (1) for obtaining approximate solutions in media with spatially varying dielectric permittivity. When reformulated as in (2) and solved using the CG method, the approach yields physically meaningful results, demonstrating its effectiveness as a computational tool.

5.2.3 Convergence

Convergence, in terms of iterations, stays reasonable both for vacuum and plasma medium, as the number of iterations is very similar.

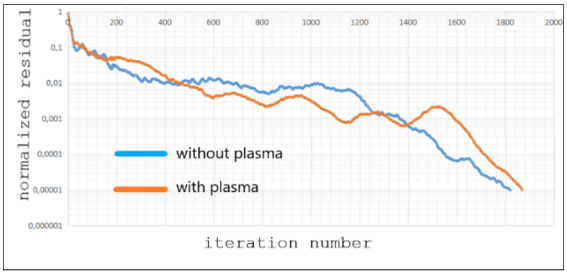

Fig. 8. Metrics of convergence for cases of vacuum and plasma.

Metric of convergence given by Figure 8 shows that convergence is achieved within reasonable number of iterations. The latter result is reasonable, since the CG method was used without a preconditioner. The scaling of the amount of calculations is given in [1]: $A=CN^{4/3}$ where C is a constant, N is the number of mesh nodes and $N^{1/3}$ represents the number of iterations (where the ideal iteration scales with $\log(N)$). Possibly, better iteration convergence rate can be achieved with application of pre-conditioning for the matrix of the system. But the price for this is more calculations at each iteration step. Moreover, some methods of pre-conditioning make complicated enabling of parallelization and SIMD instructions.

6 Conclusions

Tests of the approach with positive Maxwellian operator demonstrate numerical efficiency in solving the boundary-value problem in non-uniform plasma.

The rate of convergence of iterations is similar to the boundary-value problem in free space.

Both for vacuum and plasma cases, the computed results show the cavity mode field distribution and a visible antenna near-field.

7 Acknowledgement

This work has been carried out within the framework of the EUROfusion Consortium, funded by the European Union via the Euratom Research and Training Programme (Grant Agreement No 101052200 – EUROfusion). Views and opinions expressed are however those of the author(s) only and do not necessarily reflect those of the European Union or the European Commission. Neither the European Union nor the European Commission can be held responsible for them.

The financial support of the National Research Foundation of Ukraine (grant 2023.03/0101) is acknowledged. This study is financially supported in part by the Swedish Foundation for Strategic Research (grant UKR24-0015) and by Ministry of Education and Science of Ukraine (grant PH/ 56 - 2024).

References

1. V. E. Moiseenko & O. Ågren, Curl-free positive definite form of time-harmonic Maxwell's equations well-suitable for iterative numerical solving, Plasma Physics and Controlled Fusion **63**, 124007 (2021). https://doi.org/10.1088/1361-6587/ac32a4
2. J. Zhang et al., 2D simulation of the electromagnetic wave across the non-uniform re-entry plasma sheath with COMSOL, AIP Advances **9**, 055316 (2019). https://doi.org/10.1063/1.5085876